AGU PUBLICATIONS

Geochemistry, Geophysics, Geosystems

RESEARCH ARTICLE
10.1002/2013GC004994

Key Points:
- Foraminifer dissolution index XDX gives deep water calcite saturation
- XDX used to correct dissolution bias in Mg/Ca and shell mass records
- "Corrected" records for the core (WIND28K) are compared to published data

Supporting Information:
- Readme
- Table S1
- Figure S1

Correspondence to:
H. J. H. Johnstone,
hjohnstone@marum.de

Citation:
Johnstone, H. J. H., T. Kiefer, H. Elderfield, and M. Schulz (2014), Calcite saturation, foraminiferal test mass, and Mg/Ca-based temperatures dissolution corrected using XDX—A 150 ka record from the western Indian Ocean, *Geochem. Geophys. Geosyst.*, *15*, 781–797, doi: 10.1002/2013GC004994.

Received 12 AUG 2013
Accepted 23 JAN 2014
Accepted article online 27 JAN 2014
Published online 31 MAR 2014

Calcite saturation, foraminiferal test mass, and Mg/Ca-based temperatures dissolution corrected using XDX—A 150 ka record from the western Indian Ocean

Heather J. H. Johnstone[1], Thorsten Kiefer[2], Henry Elderfield[3], and Michael Schulz[1]

[1]MARUM—Center for Marine Environmental Sciences, University of Bremen, Bremen, Germany, [2]PAGES International Project Office, Bern, Switzerland, [3]Department of Earth Sciences, University of Cambridge, Cambridge, UK

Abstract A record of deep-sea calcite saturation ($\Delta[CO_3^{2-}]$), derived from X-ray computed tomography-based foraminifer dissolution index, XDX, was constructed for the past 150 ka for a core from the deep (4157 m) tropical western Indian Ocean. *G. sacculifer* and *N. dutertrei* recorded a similar dissolution history, consistent with the process of calcite compensation. Peaks in calcite saturation (~15 μmol/kg higher than the present-day value) occurred during deglaciations and early in MIS 3. Dissolution maxima coincided with transitions to colder stages. The mass record of *G. sacculifer* better indicated preservation than did that of *N. dutertrei* or *G. ruber*. Dissolution-corrected Mg/Ca-derived SST records, like other SST records from marginal Indian Ocean sites, showed coolest temperatures of the last 150 ka in early MIS 3, when mixed layer temperatures were ~4°C lower than present SST. Temperatures recorded by *N. dutertrei* showed the thermocline to be ~4°C colder in MIS 3 compared to the Holocene (8 ka B.P.).

1. Introduction

Surface temperatures of the tropical Indian Ocean influence the Asian Monsoon as well as the climate of Africa. A record of hydrography in this area has, therefore, great relevance to, at the least, regional-scale climate [e.g., *Leuschner and Sirocko*, 2000; *Black*, 2005]. Much of the Indian Ocean seafloor, however, lies beneath the calcite saturation horizon, meaning that sites of paleoceanographic interest have poor calcite preservation. This has implications for temperature records based on analysis of the shells of foraminifera, as partial dissolution of shell calcite at the seafloor reduces Mg/Ca, biasing-derived temperatures toward colder values [*Brown and Elderfield*, 1996; *Hastings et al*., 1998; *Dekens et al*., 2002; *Regenberg et al*., 2006].

Seafloor dissolution also reduces shell mass, a property which has been suggested as a proxy for carbonate ion concentration ($[CO_3^{2-}]$) of the surface waters where the shells form [*Barker and Elderfield*, 2002; *Naik and Naidu*, 2007; *Mekik and Raterink*, 2008; *Gonzales-Mora et al*., 2008; *Naik et al*., 2010]. Conversely, such environmental controls on shell mass confound its use as an indicator of carbonate dissolution at the seafloor [*Lohmann*, 1995; *Broecker and Clark*, 2001]. As well as indicating postdepositional bias on proxies, tracking calcite dissolution offers an insight into the past behavior of the carbon cycle, as the preservation of calcite sediments at the ocean floor records the transfer of carbon to and from the deep ocean over a glacial cycle.

The aim of this study was to create a record of calcite preservation for the south-west Indian Ocean over the past 150 ka. A temperature record covering the past 65 ka for the core used in this work, WIND28K, has been published [*Kiefer et al*., 2006]. In that study, temperatures were reconstructed from Mg/Ca of surface- (*Globigerinoides ruber* white) and thermocline- (*Neogloboquadrina dutertrei*) dwelling foraminifera. One feature of the record is the drop in Mg/Ca values during the latter part of the last glacial termination. It was noted that foraminifera tests were light in mass during this interval, suggestive of partial dissolution of the shells and consequent bias of Mg/Ca-derived temperatures.

X-ray computed tomography (CT)-based dissolution index (hereafter referred to as XDX) has been calibrated to calcite saturation ($\Delta[CO_3^{2-}]$) and to dissolution bias of Mg/Ca and of shell mass [*Johnstone et al*., 2010, 2011]. In this first down-core application of dissolution index XDX, we aim to create a record of deep water calcite saturation, and to improve shell mass and Mg/Ca-derived temperature estimates, for core WIND28K.

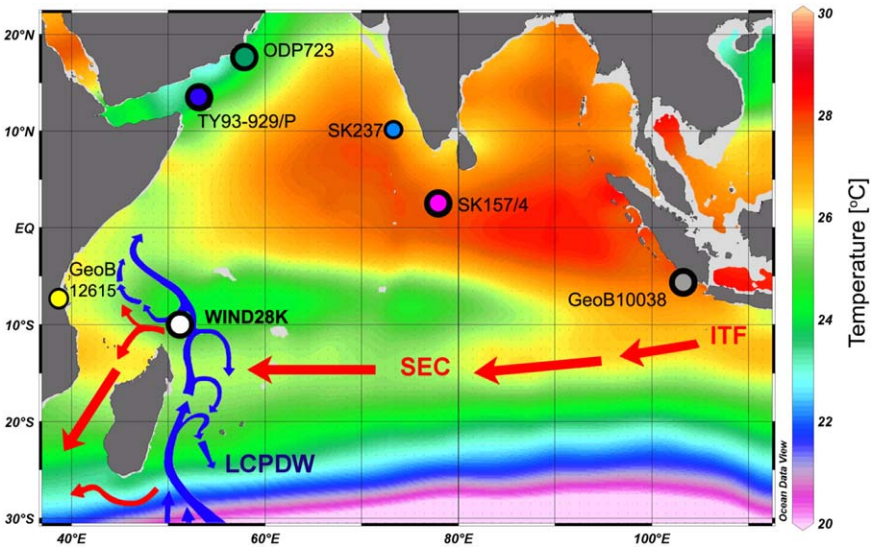

Figure 1. Location of core WIND28K [*McCave et al*., 2001] (10°9.23′S, 51°46.15′E) off Madagascar at 4157 m water depth in the Amirante Passage, Indian Ocean. Other core sites mentioned in the text (ODP723 [*Emeis et al*., 1995]; TY93-929/P [*Rostek et al*., 1997]; SK157/4 [*Saraswat et al*., 2005]; GeoB10038 [*Mohtadi et al*., 2010]; SK237 [*Saraswat et al*., 2013]; and GeoB12615 [*Romahn et al*., 2013]) are also indicated. Map colors represent annual average temperatures at 50 m water depth (World Ocean Atlas 2005 [*Locarnini et al*., 2006], plotted with Ocean Data View [*Schlitzer*, 2002, 2012]). Cool areas off the coast of Oman and to the east of WIND28K are regions of upwelling [*Schott et al*., 2009]. Blue arrows show the flow of Lower Circumpolar Deep Water (LCPDW) below 3800 m and red arrows indicate surface currents. The Indonesian Through Flow (ITF) flows east into the South Equatorial Current (SEC) which splits around Madagascar and rejoins, ultimately flowing into the Atlantic. Representation of currents is after *McCave et al*. [2005].

2. Material and Methods

2.1. Core WIND28K Location

The sediment core used in this study, WIND28K (10°09.2′S, 51°46.2′E), was collected off the north of Madagascar close to the Amirante Passage in the south-west Indian Ocean (Figure 1) [*McCave*, 2001]. Surface water at the site derives from the warm waters of the South Equatorial Current flowing from the East and cool Subantarctic Mode Water (SAMW) which upwells to the north east of Madagascar. Upwelling at this location is due to an Ekman divergence associated with the termination of the NE trade winds. Upwelling can form during both monsoon seasons but is strongest during the SW monsoon (June-September) [*Schott et al*., 2002, 2009]. Surface temperatures at the site thus have a large seasonal variation ranging from 24°C (August) to 27.5°C (March) [*Slutz et al*., 1985].

The WIND28K site lies 4157 m below the sea surface in the Lower Circumpolar Deep Water (LCPDW). This dense cold water, formed mainly on the coastal shelf around Antarctica, is the north flowing extension of Antarctic Bottom Water (AABW). Poor calcite preservation at site WIND28K would be expected, as these waters are undersaturated with respect to calcite. All calcite saturation values referred to in this paper are in the form of $\Delta[CO_3^{2-}]$, where:

$$\Delta[CO_3^{2-}] = [CO_3^{2-}]_{IN\ SITU} - [CO_3^{2-}]_{SAT}$$

$[CO_3^{2-}]_{IN\ SITU}$ is the $[CO_3^{2-}]$ value at a site and $[CO_3^{2-}]_{SAT}$ is the theoretical value of $[CO_3^{2-}]$ for calcite saturation at the site. Present-day $\Delta[CO_3^{2-}]$ of bottom water at the WIND28K site , calculated with CO2SYS [*Pierrot et al*., 2006] using total carbon and alkalinity values from GLODAP [*Key et al*., 2004] and temperature values from World Ocean Atlas 2005 [*Locarnini et al*., 2006], is -11 μmol/kg.

2.2. Age Model for Core WIND28K

Age control of sediment core WIND28K is based on 10 monospecific planktonic radiocarbon dates and benthic $\delta^{18}O$. More details of the age model are given in supporting information (Figure S1 and Table S1). The most recent radiocarbon date (from 0 to 1 cm in the core) gave an age older than the sample at 20–21

cm, indicating a disturbance in the upper 20 cm of the core. Only the part of the core older than this (8 ka B.P.) was interpreted. The age of the other dated samples increased with depth. Sedimentation rate varied from 2.4 to 6.4 cm/ka with an average rate of 4.1 cm/ka.

2.3. Foraminiferal Records

Stable isotopes (δ^{13}C and δ^{18}O) of *Cibicidoides wuellerstorfi*, *G. ruber* (white), and *N. dutertrei*, and also Mg/Ca and test mass for the two latter species, have been published for the past 65 ka by *Kiefer et al*. [2006]. Those records are extended here to 150 ka and are supplemented by data for *Globigerinoides sacculifer* (without a final sac-like chamber). Shell mass was based on at least 20 shells picked from the 300 to 355 μm size fraction weighed on a microbalance. Ideally, 50–70 shells were weighed to ensure statistical reproducibility, but some core slices contained fewer than this number. *G. ruber* and *N. dutertrei* mass was measured every 2 or 4 cm throughout all 622 cm of core WIND28K. *G. sacculifer* mass was measured every 2 or 4 cm over the glacial terminations and at lower resolution, of 8–12 cm, between these events.

For stable isotopes, *C. wuellerstorfi* was sampled every 4 cm throughout core WIND28K (162 samples). For *G. ruber*, sampling was every 2 cm in the first 76 cm of core and every 4 cm thereafter until 560 cm (139 samples). For *G. sacculifer*, stable isotopes were measured only over the glacial terminations (20–79 and 527–560 cm) with a sample step of 4 cm (37 samples). For *N. dutertrei*, stable isotope samples were analyzed every 4 cm between 20 and 560 cm in the core (134 samples). Samples where only stable isotopes were to be analyzed consisted of six specimens. Where Mg/Ca was also required, samples consisted of at least 15, and preferably 40, tests which were crushed and mixed, then a subsample, usually around a quarter of the whole, was split off for isotope analysis. Stable isotopes were analyzed on a Micromass SIRA dual inlet mass spectrometer at the Godwin Laboratory, University of Cambridge where long term precision is within $\pm 0.08‰$ (1σ) for δ^{18}O and $\pm 0.06‰$ (1σ) for δ^{13}C.

For trace metal analysis (Mg/Ca), *G. ruber* and *N. dutertrei* samples were analyzed every 4 cm where samples allowed, giving 110 analyses of *G. ruber* (from between 20 and 540 cm in the core) and 115 *N. dutertrei* analyses (from 20 to 560 cm). *G. sacculifer* was sampled every 4 cm over the glacial terminations and every 8 or 12 cm between these events (giving 76 Mg/Ca analyses between 20 and 530 cm in the core). Samples only for trace metals, where no isotope sample was run, consisted of 10–30 tests. Crushed tests were cleaned according to the method of *Barker et al*. [2003]. Most of the Mg/Ca data were generated at University of Cambridge in 2004 using a Varian Vista ICP-OES (inductively coupled plasma-optical emission spectroscopy) and Mg/Ca ratio intensity method [*de Villiers et al*., 2002]. Additional Mg/Ca samples analyzed for the current study were measured by Finnigan Element II ICP-Mass Spectrometry (ICP-MS) at MARUM, University of Bremen. Duplicate measurements in the two laboratories established that there was an offset of 0.26 mmol/mol between the two sample sets. This is within the range of measurement differences found by *Rosenthal et al*. [2004] for samples of *G. sacculifer* cleaned and analyzed in different laboratories, and is probably due to differences in calibration standards. (At the time these samples were analyzed, the use of certified limestones as external standards suggested by *Greaves et al*. [2005] had not been routinely adopted.) Mg/Ca values obtained in Bremen were adjusted by $+0.26$ mmol/mol to match those measured in Cambridge. Al, Fe, and Mn were measured in addition to Mg and Ca in order to monitor contaminants. Reproducibility in Mg/Ca-derived temperatures, due to analytical error and sample inhomogeneity, was assumed to be $\pm 0.5°$C, as estimated by *Kiefer et al*. [2006] for WIND28K samples. This is a common estimate of uncertainty for Mg/Ca paleotemperature reconstructions [*Barker et al*., 2003; *Anand and Elderfield*, 2005].

2.4. Calibration of Mg/Ca to Temperature

For greatest accuracy, calibrations between Mg/Ca and temperature would be obtained from samples from the same location, cleaned using the same method, as the samples to be calibrated. Ideally, calibrations would also be based on foraminifera of the same size fraction, as there is some evidence to suggest that Mg/Ca is sensitive to size in, at least some species of, planktonic foraminifera [*Elderfield et al*., 2002; *Friedrich et al*., 2012].

For *G. ruber* (white), the calibration of *Anand et al*. [2003] for the 250–350 μm size range meets most of the above criteria, and therefore, this equation was used:

$$\mathrm{Mg/Ca} = 0.34\ (\pm 0.08)\ \exp\ (0.102\ (\pm 0.010)\ *\ \mathrm{T})$$

For *G. sacculifer*, the calibration of *Nuernberg et al*. [2000], which is based on *G. sacculifer* (without sac) in the 250–500 μm size range, cleaned using the same cleaning method as the WIND28K samples, was used:

$$\mathrm{Mg/Ca} = 0.491\ \exp\ (0.076\ *\ \mathrm{T})$$

Several calibration equations exist for *N. dutertrei*. The calibrations of *Dekens et al*. [2002] and *Regenberg et al*. [2009] are for the same size fraction as the WIND28K samples, but use the harsher (reductive) cleaning method of *Boyle* [1981] which decreases Mg/Ca in shells. The calibration of *Anand et al*. [2003] was based on the same cleaning method as that used in this study, but is for a slightly different size range (350–500 μm) to that of the WIND28K samples (300–355 μm). However, there is presently no evidence that shell size of this species affects its Mg/Ca. For consistency with *Kiefer et al*. [2006], the calibration of *Anand et al*. [2003] was used for *N. dutertrei*:

$$\mathrm{Mg/Ca} = 0.342\ (\pm 0.012)\ \exp\ (0.090\ *\ \mathrm{T}).$$

2.5. X-Ray Computed Tomography-Based Dissolution Index, XDX

Computed tomography (CT) is a nondestructive imaging technique which uses (in this case) X-rays to map the internal structure of objects. A study of planktonic foraminifera [*Johnstone et al*., 2010] from sediment surface samples, where $\Delta[CO_3^{2-}]$ ranged from 40 to −20 μmol/kg, shows that progressive features of dissolution can be seen CT scans. Dissolution index, XDX, is an empirical method of assessing preservation state based on these dissolution features. XDX consists of five stages, from XDX of 0, where tests are very well preserved, to XDX of 4, where the inner test has mostly dissolved. Although the index is subjective—different researchers can categorize the same CT scan differently—a test of 10 people found the record of dissolution produced by different researchers to be similar. More details of the method can be found in *Johnstone et al*. [2010].

To create XDX data for core WIND28K, *G. sacculifer* (without a final sac-like chamber) and *N. dutertrei* tests were picked from washed sediment of the 300–355 μm size fraction. Tests were rinsed in deionized water and whirled for a few minutes in a vortex mixer in an attempt to remove loose sediment from inside the chambers. Samples were then dried in a warm oven before being scanned. This size fraction and preparation were selected in order to be consistent with the calibration samples of *Johnstone et al*. [2010].

Samples were scanned using a Skyscan 1072 X-ray micro-CT system. Voltage was 80 kV and exposure time was 4.5 s following the method of *Johnstone et al*. [2010]. Foraminifera were scanned in batches of 8–12 tests. Two or three batches were scanned for each sample, giving a total of 20–30 scanned tests for each sampled depth. Each test was assigned an XDX value. These were averaged to give one XDX value for each sample (Figure 2). All XDX categories were assigned by the same person (HJ). About half of the *G. sacculifer* samples were scanned at the Department of Earth Sciences, University of Cambridge, UK. The rest of the *G. sacculifer* and the *N. dutertrei* samples were scanned at the Alfred Wegener Institute for Polar and Marine Research in Bremerhaven, Germany.

The record of XDX for WIND28K was sampled at a lower resolution than the records of Mg/Ca and test mass. Resolution of 2000–3000 years should be adequate to capture the main interglacial-glacial features of bottom water calcite saturation. The higher-resolution records were linearly interpolated between data points to put them on the XDX scale. *G. sacculifer* was scanned every 8–12 cm over the first 540 cm of core WIND28K, giving 52 samples (49 of which had Mg/Ca data, Mg/Ca was interpolated for three XDX data points). *N. dutertrei* was scanned every 10 cm over the whole 622 cm of the core and some additional samples were added later, giving 74 samples in total (of which 43 depths had Mg/Ca values, 31 Mg/Ca values were interpolated).

2.6. Estimate of $\Delta[CO_3^{2-}]$, Dissolution-Corrected Mg/Ca, and Dissolution-Corrected Shell Mass From XDX

Conversion of XDX values to estimates of calcite saturation ($\Delta[CO_3^{2-}]$), predissolution shell mass and predissolution Mg/Ca are based on published calibrations [*Johnstone et al*., 2010, 2011]. Core tops used in the

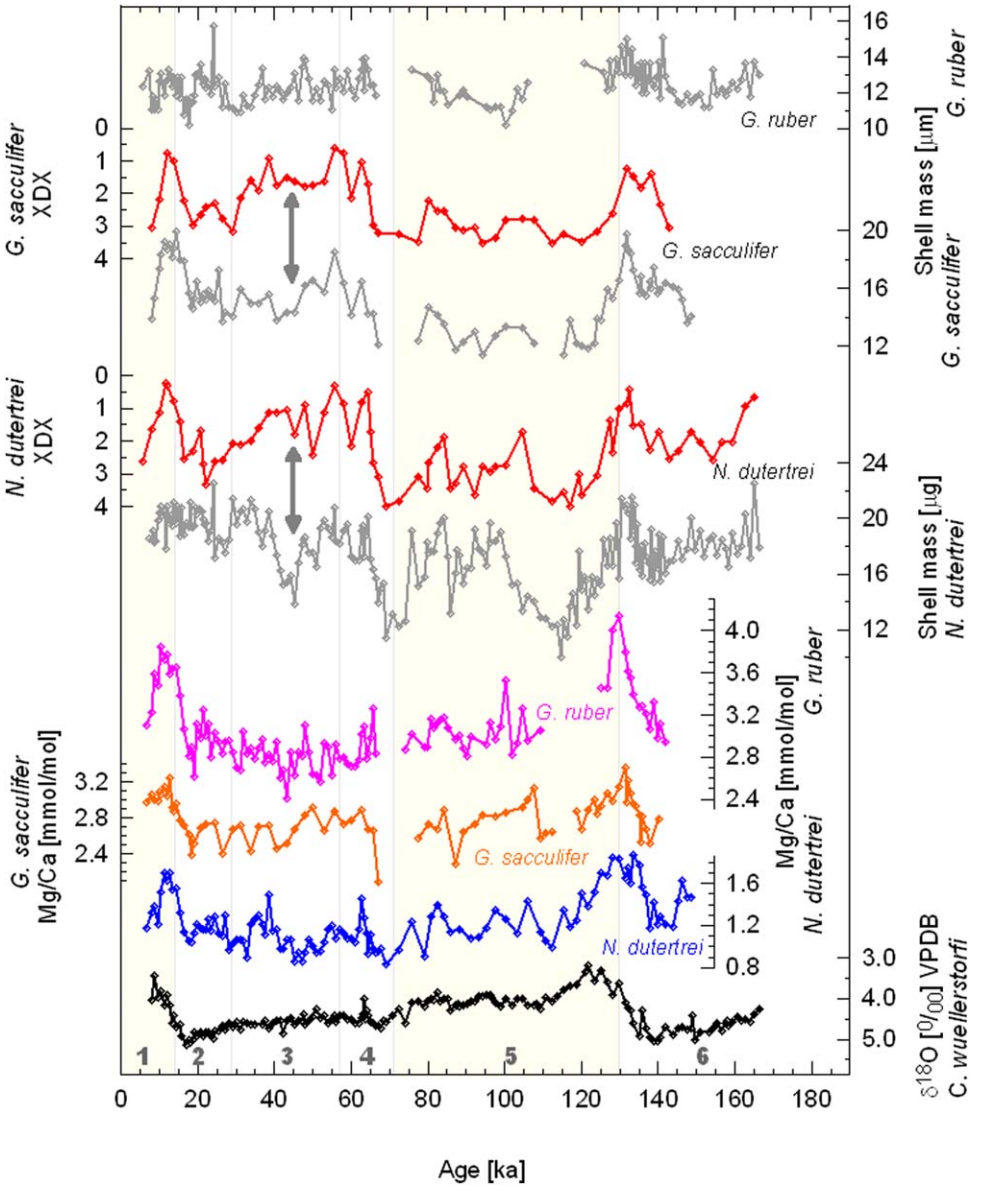

Figure 2. XDX, measured shell mass, and measured Mg/Ca for three species of planktonic foraminifera from core WIND28K. Gray lines are measured shell mass records for *G. ruber*, *G. Sacculifer*, and *N. dutertrei* as marked. Red lines are dissolution index XDX for *G. sacculifer* and *N. dutertrei* (better preservation is up axis for both mass and XDX). Gray arrows at ~42 ka, mark an interval where tests are light in weight despite reasonably good preservation. Measured Mg/Ca for *G. ruber* white (pink line); *G. sacculifer* (orange); *N. dutertrei* (blue) is shown. Black curve is benthic $\delta^{18}O$ measured on *C. wuellerstorfi*. Numbers 1–6 mark MIS [*Lisiecki and Raymo*, 2005] and vertical pale yellow bars indicate warm stages.

calibration studies included box cores from part of the WIND cruise transect [*McCave*, 2001] along the East coast of Madagascar from where core WIND28K was also retrieved.

$\Delta[CO_3^{2-}]$ was estimated from XDX of *G. sacculifer* and of *N. dutertrei*, according to:

$$\Delta\left[CO_3^{2-}\right] = a * \ XDX + b \tag{1}$$

Where *a* and *b* are species specific constants (given in Table 1 for *G. sacculifer* and *N. dutertrei*).

For Mg/Ca and shell mass, estimates of the dissolved portion added to the measured value provide an estimate of the initial, predissolution, value.

Table 1. Constants for Calibrations Between XDX and $\Delta[CO_3^{2-}]$ (equation (1)); XDX and ΔMg/Ca (equations (2) and (4)); and XDX and ΔM (equations (3) and (5)) [*Johnstone et al.*, 2010, 2011][a]

	$\Delta[CO_3^{2-}]$		ΔMg/Ca			ΔM		
Species	*a*	*b*	*c*	*d*	*f*	*g*	*h*	*m*
G. ruber			10 (±4)	13 (±4)		3 (±2)	16 (±7)	
G. sacculifer	−8 (±1)	14 (±3)			0.28 (±0.05)			3.5 (±0.4)
N. dutertrei	−8 (±1)	13 (±3)			0.29 (±0.04)			3.0 (±0.4)

[a]± is 1σ. *b* is the $\Delta[CO_3^{2-}]$ value where XDX = 0, i.e., dissolution is first detected below this value of calcite saturation. *d* is the $\Delta[CO_3^{2-}]$ value where (i.e., ΔMg/Ca = 0) Mg/Ca of *G. ruber* is first affected by dissolution. *h* is the $\Delta[CO_3^{2-}]$ value where (i.e., Δmass = 0) test mass of *G. ruber* is first affected by dissolution.

Estimate of initial, predissolution, Mg/Ca from XDX is given by:

$$Mg/Ca_{INITIAL} = Mg/Ca_{MEASURED} + \Delta Mg/Ca \quad (2)$$

Where $Mg/Ca_{MEASURED}$ is the analyzed value and ΔMg/Ca is postdeposition reduction in Mg/Ca.

ΔMg/Ca was calculated from XDX of *G. sacculifer* and of *N. dutertrei* using:

$$\Delta Mg/Ca = f * XDX \quad (3)$$

Where *f* is a species specific constant (given in Table 1 for *G. sacculifer* and *N. dutertrei*).

Estimate of initial, predissolution, shell mass from XDX is given by:

$$Mass_{INITIAL} = Mass_{MEASURED} + \Delta M \quad (4)$$

Where $Mass_{MEASURED}$ is the average measured mass of a shell and ΔM is the estimate of the dissolved portion.

ΔM was calculated from XDX of *G. sacculifer* and of *N. dutertrei* according to

$$\Delta M = m * XDX \quad (5)$$

Where *m* is a species specific constant (given in Table 1 for *G. sacculifer* and *N. dutertrei*).

XDX was not measured on *G. ruber* for two reasons. In the calibration study of *Johnstone et al*. [2010], dissolution stages were more difficult to identify in *G. ruber* than in species with a robust outer crust. Correlation between XDX of *G. ruber* and $\Delta[CO_3^{2-}]$ (r^2 of 0.4) was the lowest for the species examined. Another reason for not scanning *G. ruber* was that specimens were sparse in remaining WIND28K samples, particularly from dissolved sections.

For *G. ruber*, $\Delta[CO_3^{2-}]$ values calculated from XDX of *G. sacculifer* ($\Delta[CO_3^{2-}]_{SACC}$) were used to estimate ΔMg/Ca and ΔM. XDX values obtained from *G. sacculifer* rather than *N. dutertrei* were used as an estimate of *G. ruber* preservation as the dissolution susceptibility of *G. ruber* is more similar to that of *G. sacculifer* than to *N. dutertrei* [*Berger*, 1970].

ΔMg/Ca was calculated for *G. ruber* according to:

$$\Delta Mg/Ca = \left(\Delta[CO_3^{2-}]_{SACC} - d\right)/c \quad (6)$$

ΔM was calculated for *G. ruber* according to:

$$\Delta M = \left(\Delta[CO_3^{2-}]_{SACC} - h\right)/g \quad (7)$$

d and *h* are the threshold values of $\Delta[CO_3^{2-}]$ above which no dissolution effect on mass [*Johnstone et al.*, 2010], or Mg/Ca [*Johnstone et al.*, 2011], respectively, is detected. For samples, where $\Delta[CO_3^{2-}]_{SACC}$ was greater than the threshold value, no adjustment to measured mass or Mg/Ca was made. Values of constants

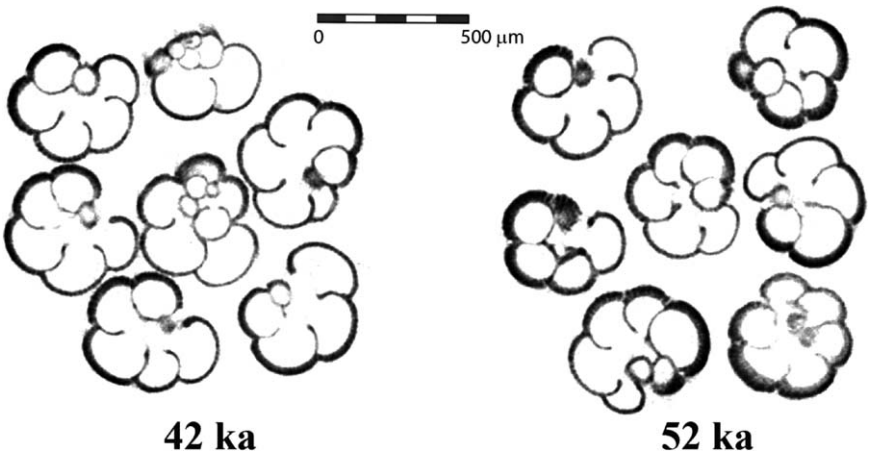

Figure 3. CT slice of *N. dutertrei* samples from (left) 42 ka, where average test mass is 14 μg, and (right) 52 ka where average test mass is 20 μg. Both samples are reasonably well preserved (XDX is ~1) but the tests from 42 ka formed with thinner walls.

are given in Table 1. For *G. ruber*, the estimate of initial, predissolution, Mg/Ca was then obtained using equation (2) and the estimate of initial, predissolution, mass was obtained using equation (4).

3. Results and Discussion

3.1. Dissolution Recorded in Core WIND28K

XDX of the two species scanned, *G. sacculifer* and *N. dutertrei* (Figure 2), showed a similar pattern of dissolution ($r^2 = 0.70$, $p < 0.001$), with good preservation (XDX <1) only over the glacial terminations and during Marine oxygen isotope stage (MIS) 3. Foraminiferal test mass is a commonly used measure of dissolution [*Lohmann*, 1995; *Broecker and Clark*, 2001, 2002a, 2000b] and test mass records for *G. sacculifer* and *N. dutertrei* show similarities to dissolution record XDX in WIND28K (Figure 2). Stronger correlation between XDX and test mass for *G. sacculifer* ($r^2 = 0.56$) than for *N. dutertrei* ($r^2 = 0.40$) suggests that mass of *G. sacculifer* is the better gauge of dissolution at this site. Correlation between XDX and measured mass is lowest for *G. ruber* (r^2 between measured mass and $XDX_{(G.\ sacculifer)}$ is 0.29, and with $XDX_{(N.\ dutertrei)}$ is 0.23). This implies that *G. ruber* mass is of limited use as a dissolution indicator at site WIND28K.

Although there are similarities between dissolution record XDX and test mass there are also significant differences. XDX assesses preservation state independently of test mass, allowing shells which are light in weight because of dissolution inside the shell, to be distinguished from well-preserved tests that are lightweight due to forming with thin walls. XDX records for *G. sacculifer* and *N. dutertrei* are more similar to each other ($r^2 = 0.70$) than the two records of test mass ($r^2 = 0.38$) implying that the record of initial (predissolution) test mass varied independently for each species over the last 150 ka. None of the three records of shell mass would suggest that preservation in MIS 3 is better than during MIS 2, as is indicated by the XDX record. In particular, there is a large deviation between test mass and XDX at ~42 ka where CT reveals that tests are well preserved but have formed with thin walls (Figure 3).

Common features in dissolution, XDX, and Mg/Ca records suggest that preservation state is also reflected in measured Mg/Ca values. Mg/Ca of all three species is highest over the glacial terminations. Lowest values occur during MIS 4 and 5e. Absence of *G. ruber* and *G. sacculifer* (the species most susceptible to dissolution [*Berger*, 1970]) over these intervals also indicates severe calcite dissolution.

3.2. Deep Water $\Delta[CO_3^{2-}]$ Reconstructed From XDX for WIND28K

3.2.1. Glacial-Interglacial Cycles in $\Delta[CO_3^{2-}]$

The calibrations between XDX and $\Delta[CO_3^{2-}]$ given in section 2.6. were used to estimate $\Delta[CO_3^{2-}]$ throughout core WIND28K (Figure 4d). $\Delta[CO_3^{2-}]$ calculated from XDX of *G. sacculifer* and from XDX of *N. dutertrei* gave similar values, with some slight differences. Maxima in $\Delta[CO_3^{2-}]$ calculated from *G. sacculifer* appeared to be 2 or 3 μmol/kg lower than values derived from *N. dutertrei*. This is within the precision of the method. Errors estimated from the uncertainty on the slope of the calibration, gave an average 1σ error of ±7.5

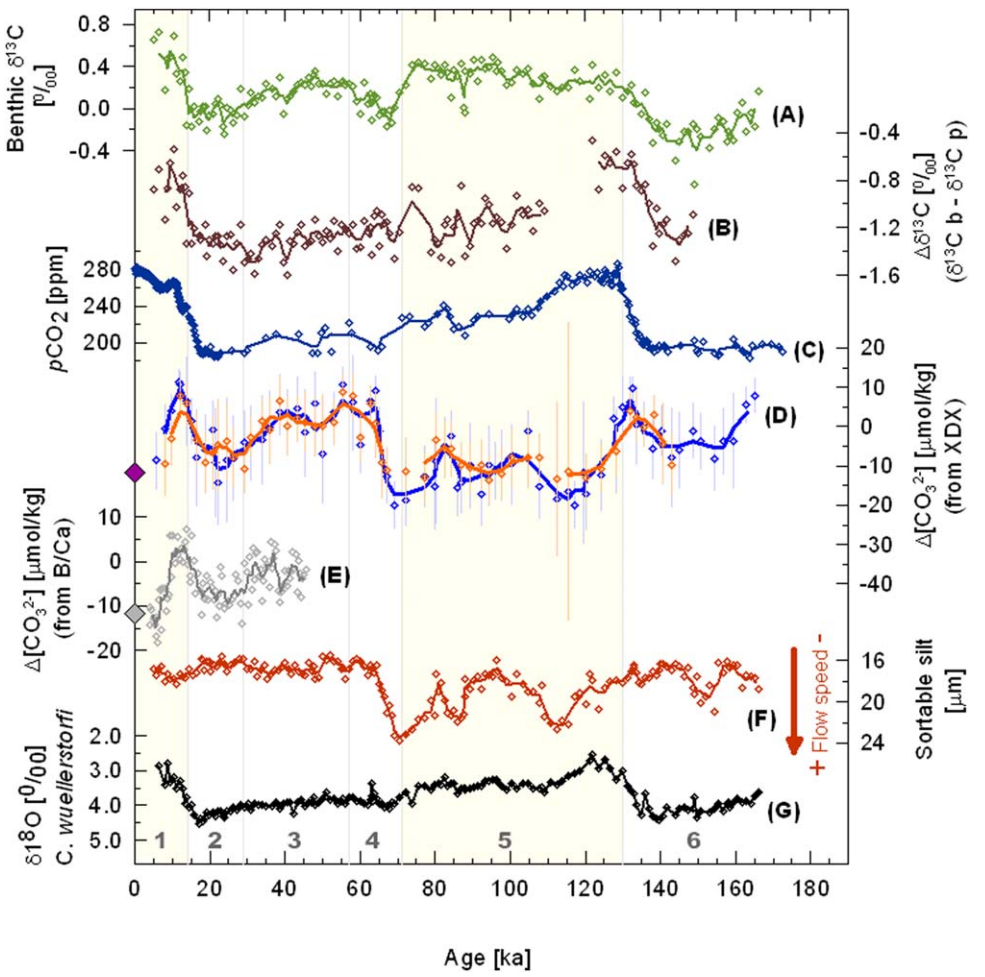

Figure 4. Deep water properties for WIND28K and atmospheric CO_2. A three point running average is plotted for each data set. (a) $\delta^{13}C$ of benthic foraminifera *C. wuellerstorfi*; (b) difference in benthic and planktic $\delta^{13}C$, $\Delta\delta^{13}C$ ($\delta^{13}C$ *C. wuellerstorfi*-$\delta^{13}C$ *G. ruber*); (c) atmospheric pCO_2 [*Petit et al*., 1999]; (d) $\Delta[CO_3^{2-}]$ derived from XDX of *N. dutertrei* (blue) and XDX of *G. sacculifer* (orange). Error bars are based on the 1σ uncertainty of the calibration slope. Purple dot indicates present-day $\Delta[CO_3^{2-}]$ [*Locarnini et al*., 2006; *Key et al*., 2004]; (e) $\Delta[CO_3^{2-}]$ derived from B/Ca of *Yu et al*. [2010]. Gray dot indicates present-day $\Delta[CO_3^{2-}]$; (f) sortable silt size which indicates flow speed (increasing downward) through the Amirante Passage [*McCave et al*., 2005]; (g) $\delta^{18}O$ of *C. wuellerstorfi*; vertical pale yellow bars indicate warm stages. Numbers 1–6 mark MIS [*Lisiecki and Raymo*, 2005].

µmol/kg on estimates of $\Delta[CO_3^{2-}]$. The difference in $\Delta[CO_3^{2-}]$ for the two species was more pronounced for the lowest values. In the WIND28K record, *N. dutertrei* indicates $\Delta[CO_3^{2-}]$ down to −20 µmol/kg, whereas *G. sacculifer* reaches minimum values of around −12 µmol/kg. These values represent the lower limits of the calibration [*Johnstone et al*., 2010]. *G. sacculifer* are less resistant to dissolution than *N. dutertrei* [e.g., *Berger*, 1970] and *G. sacculifer* tests are rare in samples from strongly undersaturated waters. The few shells found in such samples may have been better protected from dissolution in microenvironments and be may not be representative. XDX of the more robust species, *N. dutertrei* is, therefore, a better recorder of dissolution, as its tests are present in samples from a wider range of calcite saturation states. $\Delta[CO_3^{2-}]$ values calculated from *N. dutertrei* for core WIND28K ranged between values of +12 and −20 µmol/kg. Values for MIS 4 and MIS 5e were close to the limit of the *N. dutertrei* calibration range, and may not capture the full extent of undersaturation over these intervals. The most recent $\Delta[CO_3^{2-}]$ value (at 8 ka) of −13 µmol/kg was close to present-day values at the site of −11 µmol/kg.

The pattern of deep water $\Delta[CO_3^{2-}]$ recorded in WIND28K is similar to records of carbonate preservation in the deep Pacific [*Anderson et al*., 2008], and deep south Atlantic [*Hodell et al*., 2001], with best preservation, highest $\Delta[CO_3^{2-}]$, during the deglaciations and the early part of MIS 3 and poor preservation during glacial inceptions. These features are consistent with calcite compensation theory [*Broecker and Peng*, 1987], which

predicts that change in atmospheric CO_2 content is accompanied by a global change in the depth of the calcite compensation depth (CCD, the depth below which calcite is not preserved in ocean sediments). For instance, the increase in atmospheric CO_2 concentration during a deglaciation involves the transfer of CO_2 from the deep ocean to the atmosphere. This increases whole ocean $[CO_3^{2-}]$ and transient preservation events over glacial terminations have been recorded throughout the Indian and Pacific Oceans [*Berger*, 1977; *Le and Shackleton*, 1992; *Anderson et al*., 2008] as well as the deep south Atlantic [*Hodell et al*., 2001]. The northern/mid-Atlantic does not reflect these whole ocean changes as it is dominated by fluctuations in North Atlantic deep water (NADW) formation. Carbonate burial removes twice as much alkalinity as it does dissolved inorganic carbon, decreasing deep ocean $[CO_3^{2-}]$ once more until an interglacial steady state of high atmospheric CO_2 and low whole ocean $[CO_3^{2-}]$ is reached. The opposite occurs during a glacial inception, where the mixing down of CO_2 to the deep ocean acts to dissolve calcite at the seafloor. The dissolution episode at the transition from MIS 5a to MIS 4 seen in WIND28K is thought to be a global event [*Crowley*, 1983; *Broecker and Clark*, 2003].

Fluctuations in $\Delta[CO_3^{2-}]$ and $\delta^{13}C$ record changes in water mass properties at site WIND28K. Reduced formation, or shallower circulation, of NADW during cold intervals [*Sarnthein et al*., 1994; *Sigman and Boyle*, 2000] means that glacial LCPDW contains more (low $\delta^{13}C$) AABW and is, therefore, more corrosive than during warmer phases. Increased dissolution in cold intervals has been recorded in sites bathed in LCPDW in the Indian Ocean, as well as in deep sites from the Southern Atlantic Cape Basin [*Howard and Prell*, 1994; *Hodell et al*., 2001]. In the cool stages of the WIND28K record, MIS 2, 3, 4, and 6, the influence of AABW is recorded in the similarity between benthic $\delta^{13}C$ and $\Delta[CO_3^{2-}]$ (Figure 4), as has been described for the deep South Atlantic (ODP1090) record of *Hodell et al*. [2001]. Covariance between benthic $\delta^{13}C$ and $\Delta[CO_3^{2-}]$ is not seen in WIND28K during MIS 5 when $\delta^{13}C$ is generally higher. As described by *Govin et al*. [2009] for the Southern Ocean, high $\delta^{13}C$ reflects the greater NADW input during MIS 5 which reduces sharply at 70 ka.

The increased ventilation of bottom waters at the WIND28K site, described by *Yu et al*. [2010] for Termination I, is also seen during Termination II. LCPDW is a mixture of both high $[CO_3^{2-}]$, high $\delta^{13}C$ NADW and corrosive, low $[CO_3^{2-}]$, low $\delta^{13}C$ AABW. The increase in $\Delta\delta^{13}C$ ($\delta^{13}C$ of planktic (*G. ruber*)-$\delta^{13}C$ of benthic (*C. wuellerstorfi*) foraminifera) indicates that deep water is being replaced at site WIND28K by younger fresher water, with higher $\delta^{13}C$, during deglaciations (Figure 4b).

3.2.2. Estimates of Deep Ocean $\Delta[CO_3^{2-}]$ During the Past Glacial-Interglacial Cycle

The decrease in $\Delta[CO_3^{2-}]$ (calculated from XDX of *N. dutertrei*) between the Termination I maximum (at 12 ka) of 12 μmol/kg and the Holocene (8 ka) value of −13 μmol/kg is ∼25 μmol/kg. *Yu et al*. [2010] produced a record of $[CO_3^{2-}]$ for WIND28K based on B/Ca. $\Delta[CO_3^{2-}]$ was calculated from this by assuming a value of $\Delta[CO_3^{2-}]_{SAT}$ for the site of 96 μmol/kg [*Locarnini et al*., 2006; *Key et al*., 2004] and plotted in Figure 4e. Maximum $\Delta[CO_3^{2-}]$ of 6 μmol/kg at 14 ka, and minimum value of −18 at 6 ka, indicate a shift of ∼24 μmol/kg [*Yu et al*. 2010].

Marchitto et al. [2005] used Zn/Ca to estimate $\Delta[CO_3^{2-}]$ for the deep Pacific. The increase in $\Delta[CO_3^{2-}]$ for their core, RC13–114, during Termination I was 20–25 μmol/kg—very similar to the estimated $\Delta[CO_3^{2-}]$ increase for WIND28K. However, unlike the records of WIND28K (this study) [*Yu et al*., 2010], the deep South Atlantic [*Hodell et al*., 2001] and Pacific [*Anderson et al*., 2008], MIS 3 did not show higher than present-day calcite saturation. The Termination II peak in RC13–114 is smaller than that of Termination I and appears delayed in comparison with the $\delta^{18}O$ record. In contrast, maxima in $\Delta[CO_3^{2-}]$ (of +10 μmol/kg) in WIND28K are similar during Termination I, early MIS 3 and Termination II. There are known to be some problems with the Zn/Ca proxy, particularly where pore waters contain reduced Mn^{2+} [*Marchitto et al*., 2005]. The apparent differences between the Pacific, as recorded in RC13–114, and the other sites mentioned, require further understanding of the controls on Zn/Ca before they can be accepted.

$\Delta[CO_3^{2-}]$ calculated for MIS 2 in WIND28K is variable, but Last Glacial Maximum (LGM) values of −9 μmol/kg suggest that glacial $[CO_3^{2-}]$ was similar to modern values in the deep Indian Ocean, in agreement with estimates by *Anderson and Archer* [2002] and *Marchitto et al*. [2005] for the deep Pacific.

The estimates of $\Delta[CO_3^{2-}]$ for Termination I based on XDX and on trace metals (B/Ca, Zn/Ca) are more in agreement with one another than an estimate based on fragmentation of *G. menardii* shells. The Menardii Fragmentation Index (MFI) does not record any change in preservation over Termination I of core RC13–114 [*Mekik et al*., 2012] (where Zn/Ca of *Marchitto et al*. [2005] indicated a shift of 20–25 μmol/kg). For core

WIND28K, MFI shows no increase in preservation during the deglaciation, although preservation does decrease from ~16 ka [*Mekik et al*., 2012]. The pattern recorded by MFI over Termination I in WIND28K, is similar to that of the shell mass of *N. dutertrei*, which shows no change between 20 and ~10 ka, but decreases from that point on (Figure 2). *Mekik et al*. [2012] suggest the failure of MFI to record preservation peaks is due to changes in shell thickness, meaning that fragmentation may be more or less likely for the same degree of calcite undersaturation. The fact that XDX records $\Delta[CO_3^{2-}]$, despite such changes in shell thickness gives confidence in XDX as a $\Delta[CO_3^{2-}]$ proxy.

3.2.3. Local Factors With Potential to Affect $\Delta[CO_3^{2-}]$ Record of WIND28K

Degradation of organic matter can mean that sediment pore waters are more corrosive than overlying deep water [*Emerson and Bender*, 1981; *Hales and Emerson*, 1997]. Records of calcite preservation and C_{org} have been found to covary at shallow coastal sites where seasonal upwelling enhances productivity [*Bassinot et al*., 1994; *Kloecker et al*., 2006]. However, the open ocean upwelling near the WIND28K site is not associated with large changes in productivity. Chlorophyll concentration increases only slightly, from 0.1 mg/m^3 in winter to 0.2 mg/m^3 in summer [SEAWIFS Ocean color database, http://Oceancolor.gsfc.nasa.gov]. Neither is there depletion of $\delta^{13}C$ in surface waters during periods of strong monsoon, which would indicate upwelling enhanced productivity [*Beaufort et al*., 1997] at WIND28K. For these reasons, we consider the degradation of organic matter to play an insignificant role in carbonate dissolution at WIND28K.

One factor which may have imposed a local signal on calcite preservation is the variation in flow speed through the Amirante Passage on glacial to interglacial time scales [*McCave et al*., 2005]. Periods of global cooling and falling sea level result in faster flow through the Amirante Passage. This is indicated by increases in sortable silt size at transitions from MIS 5a to 4; 5e to 5d and 6e to 6d [*McCave et al*., 2005]. These peaks in sortable silt size (Figure 4f) correspond with episodes of poor calcite preservation. It may be that the increased winnowing of the fine-grained fraction from the sediment during episodes of faster flow reduces protection by clays and increases exposure time of tests to corrosive deep water.

3.3. Dissolution-Corrected Temperature Record in WIND28K

3.3.1. Sea Surface Temperatures

The calibrations given in sections 2.4. and 2.6. were used to estimate initial, prealteration, Mg/Ca-based temperatures. Temperatures derived from *G. ruber* in core WIND28K increased from analyzed values of 19–24°C to XDX-corrected values of 22–28°C. These corrected values are within the range of peak abundance for this species of 21–29°C [*Bé and Tolderlund*, 1971]. Temperatures calculated from *G. ruber* in the most recent (8 ka B.P.) samples were raised by the dissolution correction, from 22 (±0.5)°C to 27.3 (±2.4)°C. Calcification temperature of *G. ruber* is considered to represent summer SST (sea surface temperature) [*Shackleton and Vincent*, 1978]. The latter temperature appears the better estimate for SST at the WIND28K site, where annual average SST is 27.5°C and SSTs of the four warmest months are just above 28°C [*Locarnini et al*., 2006].

Temperatures represented by *G. sacculifer* are increased from a range of 19–25°C for analyzed values, to 23–27°C for XDX-corrected temperatures. This range is within its known habitat temperatures of 15–30°C [*Bé and Tolderlund*, 1971]. Like *G. ruber*, *G. sacculifer* also lives in the photic zone, but it continues to calcify deeper in the water column [*Duplessy et al*., 1981; *Rosenthal et al*., 2000]. It also has a longer season and is considered to represent annual temperatures [*Bé and Tolderlund*, 1971]. Temperatures calculated from *G. sacculifer* for the sample at 8 ka B.P. are increased from analyzed values of 24.1(±0.5)°C, to corrected values of 27.3 (±1.2)°C, which is close to modern annual average SST at the site (Figure 5).

Average temperatures (n = 6) for MIS 2 are 26.0 (±0.2)°C calculated from *G. ruber* and 25.3 (±0.3)°C from *G. sacculifer* (uncertainties are 2 times the standard error). Compared to present-day SST, MIS 2 temperatures were 1.5 (±0.2)°C and 2.2 ± (0.3)°C cooler, according to *G. ruber* and *G. sacculifer* respectively. This contrasts with temperatures calculated from foraminiferal assemblages, which indicate no change in warmest month, coolest month, or annual average temperature at the core site during the LGM compared to core-top (recent) values [*Barrows and Juggins*, 2005]. Modeled data does, however, suggest cooler temperatures at the site during the LGM. An LGM simulation (following the protocol of PMIP) [*Braconnot et al*., 2007; *Merkel et al*. 2010; U. Merkel, personal communication] show a similar seasonal pattern in SST as during preindustrial conditions, but are 1.5°C lower.

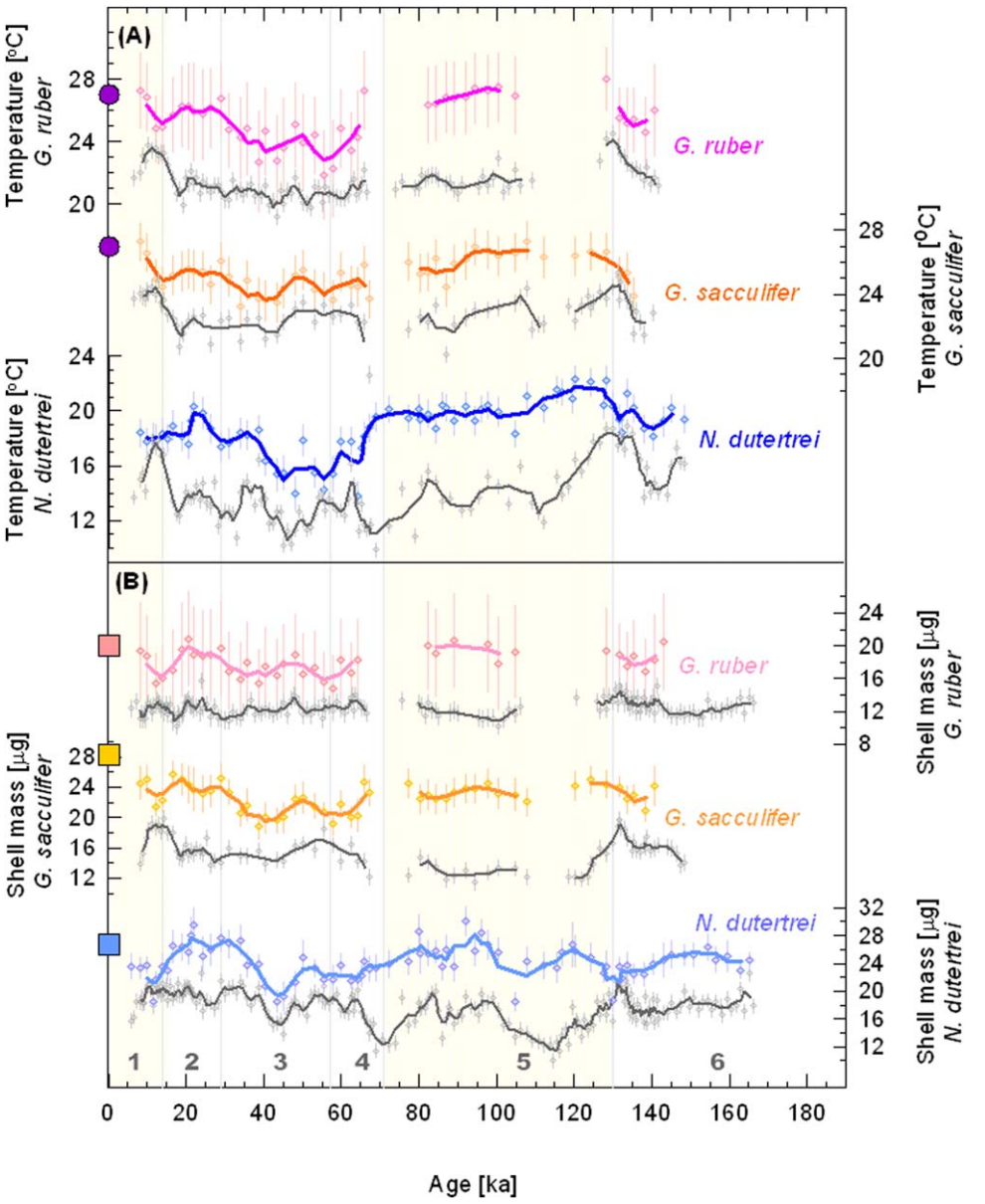

Figure 5. (a) Reconstructed, dissolution-corrected, temperatures and (b) test mass for three species of planktic foraminifera from WIND28K. Numbers 1–6 mark MIS [*Lisiecki and Raymo*, 2005]. Vertical pale yellow bars mark warm stages. (Figure 5a) Thick colored lines are three point running average of XDX-corrected Mg/Ca-based temperatures for *G. ruber* white (magenta line), *G. sacculifer* (orange), and *N. dutertrei* (blue). Gray lines for each species are three point running average of temperature estimates based on analyzed values of Mg/Ca. Error bars are ±0.5°C. Error bars on dissolution-corrected temperatures took into account the ±0.5°C uncertainty on measured temperatures and 1σ in the gradient in the calibration between XDX and ΔMg/Ca. Purple circles plotted on both the *G. ruber* and *G. sacculifer* temperature scale bars represent annual average SST [*Locarnini et al*., 2006] at WIND28K site. (Figure 5b) Thick solid lines are three point running average of XDX-corrected shell mass for *G. ruber* white (pink line), *G. sacculifer* (orange line), and *N. dutertrei* (blue line). Gray lines for each species are three point running average of measured mass. Uncertainty was assumed to be ±0.5 µg on measured mass. Error bars on dissolution-corrected mass took into account uncertainty on the measured values and 1σ in the gradient in the calibration between XDX and ΔMass. Colored squares represent average mass of tests from core-tops (WIND10B, WIND11B) from shallow sites in the Western Indian Ocean [*Johnstone et al*., 2010].

SST reconstructed for WIND28K differs from published records from the equatorial Indian Ocean. Such records [*Bard et al*., 1997; *Saraswat et al*., 2005] (Figure 6), like those from the Eastern equatorial Pacific [*Lea et al*., 2000], show a pattern similar to that of high-latitude temperatures over the last 150 ka, where MIS 2 and MIS 4 temperatures are slightly cooler than those of MIS 3, and warmest temperatures occur in MIS 5.5. The dissolution-corrected WIND28K record (Figure 6) showed warmest SSTs in the Holocene and during MIS 5e, while coolest temperatures of the past 150 ka were early in MIS 3. Average temperatures for MIS 3

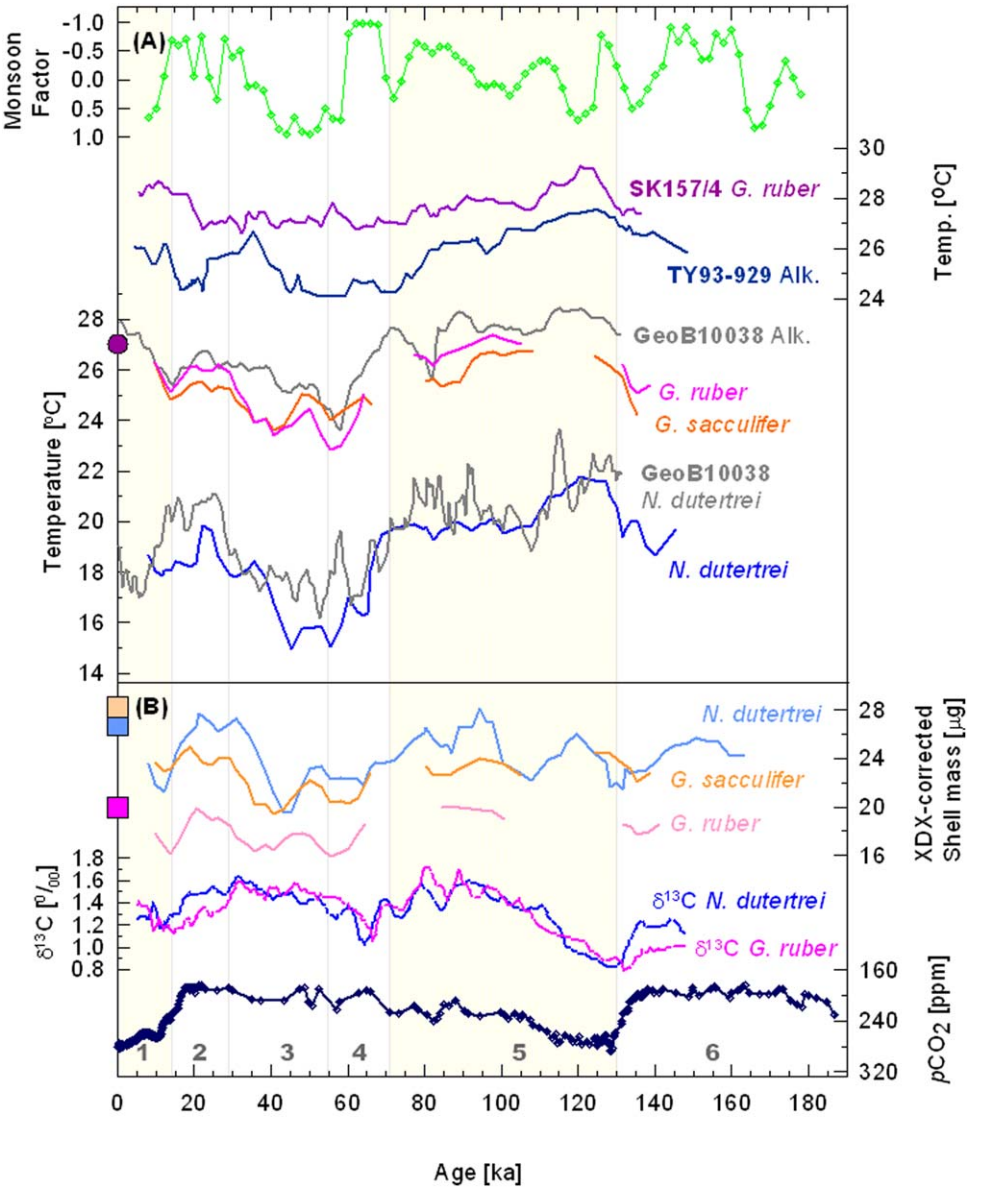

Figure 6. Dissolution-corrected shell mass and temperature records for WIND28K and comparison with published records.(a) Green line is Monsoon Factor of *Clemens and Prell* [2003] (strength of SW monsoon increases downward). Plots where individual data points are not shown are three point running averages. Purple line is SST based on *G. ruber* from SK157/4 [*Saraswat et al.*, 2005] in the Indian Ocean and blue line is SST derived from alkenones for TY93–929/P [*Rostek et al.*, 1997] from the Arabian Sea. Alkenone-based SST record from east Indian Ocean core GeoB10038-4 [*Mohtadi et al.*, 2010] (light gray line) is plotted on the same scale as temperatures derived from *G. ruber* white (magenta line) and *G. sacculifer* (orange line) of WIND28K. Purple circles are annual average SST at WIND28K site, as in Figure 4. Thermocline temperatures based on Mg/Ca of *N. dutertrei* are shown for GeoB10038-4 [*Mohtadi et al.*, 2010] (dark gray line) and WIND28K (blue line). (b) Reconstructed test mass for *N. dutertrei* (light blue line), *G. sacculifer* (light orange line), and *G. ruber* white (pink line) from WIND28K. Colored squares represent mass of tests from shallow sites in the Western Indian Ocean, as in Figure 5. δ^{13}C of planktonic foraminifera from WIND28K is shown for *G. ruber* (thin dashed pink line), and *N. dutertrei* (thin dashed blue line). pCO_2 (black line) is plotted on inverse scale, as an approximation of surface water $[CO_3^{2-}]$. Numbers 1–6 mark MIS [*Lisiecki and Raymo*, 2005] and vertical pale yellow bars mark warm stages.

(n = 12) were 24.5 (±0.5)°C and 24.1 (±0.7)°C calculated from *G. ruber* and *G. sacculifer*, respectively, suggesting that the mixed layer was ~3°C cooler than at present during MIS 3. These temperatures are lower than those of MIS 2, and not significantly higher than the average for MIS 4 (24.8 (±1.5)°C from *G. ruber*; 24.6 (±0.7)°C from *G. sacculifer*, n = 6).

Dissolution correction of WIND28K SST removes the apparent drop in temperature during Termination I, at 12 ka. In the corrected record, *G. ruber* and *G. sacculifer* show steady warming through MIS 1. The large

uncertainty on dissolution-corrected temperatures does not allow precise identification of the start of deglacial warming. Taking the results at face value, warming is late in comparison both to δ^{18}O of benthic foraminifera from WIND28K and in comparison to published records from the tropics. Neither SST nor thermocline temperatures of WIND28K follow the pattern of continuous warming from 19 ka identified by *Kiefer and Kienast* [2005] for the central Pacific. Two new high-resolution SST reconstructions for the Indian Ocean (cores GeoB12615 [*Romahn et al*., 2013] and SK237 [*Saraswat et al*., 2013]) suggest that the Indian Ocean also warmed from ~19 ka B.P., although not continuously, but in two steps separated by a few thousand years.

Late deglacial warming, as in the WIND28K record, is, however, seen at other sites from the Indian Ocean margins. SSTs reconstructed from both alkenones and foraminiferal δ^{18}O from site ODP723 [*Emeis et al*., 1995] off Oman, and from alkenones from nearby core TY93–929/P [*Rostek et al*., 1997] (Figure 6), warm only after 15 ka B.P. Both these records, like WIND28K, have cool temperatures at the beginning of MIS 3. An alkenone-based SST record from core GeoB10038-4 [*Mohtadi et al*., 2010] from the Eastern Indian Ocean near Sumatra shows warming only after 12 ka and has coolest SST of the last 135 ka at the start of MIS 3. Both these areas, off Oman and off Sumatra, are subject to upwelling during the boreal summer monsoon season. Changes in upwelling intensity probably contribute to the cold temperatures during MIS 3, when the SW monsoon is particularly strong in the Arabian Sea [*Clemens and Prell*, 2003] (Figure 6). Not all of the temperature change may be attributable to upwelling. As described by *Emeis et al*. [1995] and *Rostek et al*. [1993], some SST records from nonupwelling areas in the Indian Ocean also show cooler temperatures during MIS 3. They attribute this to a basin-wide change in conditions connected with the strength of the monsoon system.

3.3.2. Thermocline Temperatures

The greater sensitivity to the effect of dissolution on temperatures derived from Mg/Ca of *N. dutertrei* compared to the other species considered [*Fehrenbacher et al*., 2006; *Regenberg et al*., 2006; *Johnstone et al*., 2011], means that dissolution correction causes the largest temperature adjustment in this species. *N. dutertrei* also has the largest temperature range of the three species, presumably reflecting its wider habitat depth range [*Hemleben et al*., 1989]. Reconstructed temperatures increased from a range of 10–19°C for analyzed values to 14–22°C for XDX-corrected values. XDX-corrected temperatures at the top of the core (~8 ka) of 18.5°C would represent a calcification depth in the lower part of the thermocline, according to the modern-day temperature profile [*Locarnini et al*., 2006], in keeping with the known habitat of this species [*Hemleben et al*., 1989; *Bé and Tolderlund*, 1971].

Dissolution-corrected thermocline temperatures in WIND28K are similar to those of core GeoB10038-4 from off Sumatra in the East Indian Ocean [*Mohtadi et al*., 2010] (Figure 6). In that study the authors note the similarity with thermocline data of *Budziak et al*. [2000] from the Western Arabian Sea. Despite potential moderation by inputs of Red Sea and Persian Gulf water, records of thermocline temperatures in the Indian Ocean for the last glacial cycle appear to be similar over a wide area.

3.4. Dissolution-Corrected Test Mass

Test mass records for *G. sacculifer* and *N. dutertrei* were reconstructed using XDX according to equations (5) and (4) and *G. ruber* mass was reconstructed using equations (7) and (4) (section 2.4.). Mass of *G. ruber* was increased from a range of 10–16 to 15–23 μg. Mass of *G. sacculifer* was increased from 11–20 to 19–26 μg. *N. dutertrei* mass increased from a range of 10–23 to of 19–30 μg. Dissolution-corrected test mass of the most recent samples (8 ka B.P.) was more similar to that of well-preserved (XDX < 1) samples from the region (core top samples WIND10B, WIND11B [*Johnstone et al*., 2010]), than was the uncorrected mass (Figure 5).

One problem with any potential dissolution correction is that if a parameter reaches a baseline value, such that the variability in the original signal is lost, then the record can no longer be corrected. "Corrected" values would be underestimates, on average, and the record would resemble the inverse of the correction factor. *Johnstone et al*. [2010] observe that partially dissolved shells, from the 300 to 355 μg size fraction, reach a minimum mass of ~12 μg for *G. sacculifer* and *N. dutertrei*, and ~11 μg for *G. ruber*. Further dissolution results in fragmentation of the test, not loss of mass. Data from WIND28K supported this observation. Few samples of *G. ruber* weighed less than 11 μg (Figure 5). Average mass of *G. ruber* is 12 (±1) μg (the number in brackets was calculated as 1σ, although in fact it is a positively skewed distribution). Correlation between the *G. ruber* mass and $XDX_{(G.\ sacculifer)}$ ($r^2 = 0.16$) was much lower than correlation between "dissolution-corrected" *G. ruber* mass and $XDX_{(G.\ sacculifer)}$, where $r^2 = 0.75$. It appears therefore that the dissolution-

corrected mass record of *G. ruber* is unreliable and that the apparent sharp 4 μg drops in shell mass, coincident with preservation maxima during the glacial terminations, may be an artefact of the good preservation during these intervals.

The heavier shells of *G. sacculifer* and *N. dutertrei* species, although partially dissolved, retain more of the original variability in their shell mass records. For both these species, correlation between XDX and mass was greater for the measured record than for the corrected record. Correlation (r^2) between $XDX_{(G.\ sacculifer)}$ and measured shell mass (uncorrected for dissolution) is 0.64. Correlation (r^2) between $XDX_{(G.\ sacculifer)}$ and XDX-corrected mass is 0.52. For *N. dutertrei*, the values are r^2 of 0.39 between $XDX_{(N.\ dutertrei)}$ and measured shell mass, and r^2 of 0.34 between $XDX_{(N.\ dutertrei)}$ and XDX-corrected mass.

The mass of planktic foraminifera tests has been related to sea water parameters, particularly carbonate ion concentration ($[CO_3^{2-}]$), during calcification [*Spero et al*., 1997; *Bijma et al*., 1999; *Barker and Elderfield*, 2002; *Moy et al*., 2009]. However, the dissolution-corrected shell mass record of WIND28K shows little resemblance to the inverse of the pCO_2 curve, which would be expected if surface water $[CO_3^{2-}]$ was the main control on mass. There was a clear minimum in mass during MIS 3, although pCO_2 was relatively low at this time (Figure 6b).

Temperature exerts a relatively small control on calcite saturation [*Zeebe and Wolf-Gladrow*, 2001] but many biological reaction rates are temperature sensitive, and thus temperature may directly affect growth rate [e.g., *Gillooly et al*., 2002; *Atkinson et al*., 2003]. *Gonzalez-Mora et al*. [2008] suggest that the inverse relationship between CO_2 and mass is modified by a positive relationship between temperature and mass. The WIND28K record appears to support a temperature control on mass. Minimum (dissolution corrected) mass of *G. sacculifer* and *N. dutertrei* occurred during the coldest interval of MIS 3 (Figure 6) and CT shows shells have formed with thin walls (Figure 3). Nutrient levels may also contribute to low shell masses over this interval. *De Villiers* [2004] observed a positive relationship between nutrient availability and shell mass. $\delta^{13}C$ is relatively high (Figure 6b), suggesting low-nutrient surface waters, during the cold phase of MIS 3.

4. Conclusions

This first application of dissolution proxy XDX shows its value as an indicator of calcite saturation ($\Delta[CO_3^{2-}]$) and as a means to correct dissolution bias in Mg/Ca and in shell mass of planktic foraminifera. The pattern of calcite saturation recorded in Indian Ocean core WIND28K reflects the global reorganization of carbon between ocean and atmosphere on glacial-interglacial time scales. Bottom water was undersaturated with respect to calcite during the glacial inceptions. Highest $\Delta[CO_3^{2-}]$ values occurred during the early part of MIS 3 and during the deglaciations. The increase in $\Delta[CO_3^{2-}]$ over Termination I, of ~25 μmol/kg, calculated from XDX is similar to that of published estimates of deep ocean calcite saturation derived from B/Ca and Zn/Ca.

The dissolution-corrected temperature record of WIND28K has a pattern similar to that recorded in marginal Indian Ocean sites subject to upwelling. SST cools through MIS 4, coolest temperatures of the last 150 ka occur in MIS 3, when the SW monsoon was particularly strong, and deglacial warming was delayed in comparison to open ocean sites. The occurrence of *N. dutertrei* and *G. sacculifer* tests with thin walls and minimum (initial) mass over the cold interval in MIS 3 (when $[CO_3^{2-}]$ and $\delta^{13}C$ were relatively high) suggests that at this site, low temperature, perhaps combined with low nutrients, influenced test mass.

Acknowledgments
This project was funded through DFG Research Center/Cluster of Excellence "The Ocean in the Earth System." (FZT15/EXC309). Thanks go to Henning Kuhnert, Heiko Paelike, and Gema Martinez-Mendez for useful discussion; to Ed Hathorne and Johannes Freitag for practical assistance with analyses; and to Karen Alexander for improving the written English. The authors are grateful to Brett Metcalfe and three anonymous reviewers for useful comments which much improved this version of the manuscript.

References

Anand, P., H. Elderfield, and M. H. Conte (2003), Calibration of Mg/Ca thermometry in planktonic foraminifera from a sediment trap time series, *Paleoceanography*, *18*(2), 1050, doi:10.1029/2002PA000846.

Anand, P., and H. Elderfield, (2005), Variability of Mg/Ca and Sr/Ca between and within the planktonic foraminifers *Globigerina bulloides and Globorotalia truncatulinoides, Geochem. Geophys. Geosyst*. (6), Q11D15, doi:10.1029/2004GC000811.

Anderson, D. M., and D. Archer (2002), Glacial-interglacial stability of ocean pH inferred from foraminifer dissolution rates, *Nature*, *416*, 70–72.

Anderson, R. F., M. Q. Fleisher, Y. Lao, and G. Winckler (2008), Modern $CaCO_3$ preservation in equatorial Pacific sediments in the context of late-Pleistocene glacial cycles, *Mar. Chem.*, *111*, 30–46.

Atkinson, D., B. J. Ciotti, and D. J. S. Montagnes (2003), Protists decrease in size linearly with temperature: ca. 2.5% $°C^{-1}$, *Proc. R. Soc. London, Ser. B*, *270*, 2605–2611, doi:10.1098/rspb.2003.2538.

Bard, E., F. Rostek, and C. Sonzogni (1997), Interhemispheric synchrony of the last deglaciation inferred from alkenone palaeothermometry, *Nature*, *385*, 707–710.

Barker, S., and H. Elderfield (2002), Foraminiferal calcification response to glacial interglacial changes in atmospheric CO_2, *Science*, *297*, 833–836, doi:10.1126/science.1072815.

Barker, S., M. Greaves, and H. Elderfield (2003), A study of cleaning procedures used for foraminiferal Mg/Ca palaeothermometry, *Geochem. Geophys. Geosyst.*, *4*(9), 8407, doi:10.1029/2003GC000559.
Barrows, T., and S. Juggins (2005), Sea-surface temperatures around the Australian margin and Indian Ocean during the Last Glacial Maximum, *Quat. Sci. Rev.*, *24*, 1017–1047.
Bassinot, F. C., L. Beaufort, E. Vincent, L. D. Labeyrie, F. Rostek, P. J. Müller, X. Quidelleur, and Y. Lancelot (1994), Coarse fraction fluctuations in pelagic carbonate sediments from the tropical Indian Ocean: A 1500-kyr record of carbonate dissolution, *Paleoceanography*, *9*(4), 579–600.
Bé, A. W. H., and D. S. Tolderlund (1971), Distribution and ecology of living planktonic foraminifera in surface waters of the Atlantic and Indian oceans, in *Micropaleontology of the Oceans*, edited by B. M. Funnell and W. R. Riedel, pp. 105–149, Cambridge Univ. Press, London, pp. 105–149.
Beaufort, L., Y. Lancelot, P. Camberlin, O. Cayre, E. Vincent, F. Bassinot, and L. Labeyrie (1997), Insolation cycles as a major control of equatorial Indian Ocean primary production, *Science*, *278*(5342), 1451–1454, doi:10.1126/science.278.5342.1451.
Berger, W. H. (1970), Planktonic foraminifera: Selective solution and the lysocline, *Mar. Geol.*, *8*, 111–138.
Berger, W. H. (1977), Deep-sea carbonate and the late deglaciation preservation spike in pteropods and foraminifera, *Nature*, *269*, 301–304.
Bijma, J., H. J. Spero, and D. W. Lea (1999), Reassessing foraminiferal stable isotope geochemistry: Impact of the oceanic carbonate system (experimental results), in *Use of Proxies in Paleoceanography: Examples From the South Atlantic*, edited by G. Fischer and G. Wefer, pp. 489–512, Springer, New York.
Black, E. (2005), The relationship between Indian Ocean sea surface temperature and East African rainfall, *Philos. Trans. R. Soc. A*, *363*, 43–47.
Boyle, E. (1981), Cadmium, zinc, copper and barium in foraminifera tests, *Geochim. Cosmochim. Acta*, *47*, 1815–1819.
Braconnot, P., et al. (2007), Results of PMIP2 coupled simulations of the Mid-Holocene and Last Glacial Maximum. Part 1: Experiments and large-scale features, *Clim. Past*, *3*, 261–277.
Broecker, W. S., and E. Clark (2001), An evaluation of Lohmann's foraminifera weight dissolution index, *Paleoceanography*, *16*(5), 531–534.
Broecker, W. S., and E. Clark (2002a), Carbonate ion concentration in glacial-age deep waters of the Caribbean Sea, *Geochem. Geophys. Geosyst.*, *3*(3), doi:10.1029/2001GC000231.
Broecker, W. S., and E. Clark (2002b), Glacial-to-holocene redistribution of carbonate ion in the deep sea, *Science*, *294*, 2152–2155.
Broecker, W. S., and E. Clark (2003), $CaCO_3$ dissolution in the deep sea: Paced by insolation cycles, *Geochem. Geophys. Geosyst.*, *4*(7), 1059, doi:10.1029/2002GC000450.
Broecker, W. S., and T.-H. Peng (1987), The role of $CaCO_3$ compensation in the glacial to interglacial atmospheric CO_2 change, *Global Biogeochem. Cycles*, *1*, 15–29.
Brown, S., and H. Elderfield (1996), Variations in Mg/Ca snd Sr/Ca ratios of planktonic foraminifera caused by post depositional dissolution: Evidence of shallow Mg dependent dissolution, *Paleoceanography*, *11*(5), 543–551.
Budziak, D., R. R. Schneider, F. Rostek, P. J. Mueller, E. Bard, and G. Wefer (2000), Late Quaternary insolation forcing on total organic carbon and C37 alkenone variations in the Arabian Sea, *Paleoceanography*, *15*(3), 307–321.
Clemens, S. and W.L. Prell (2003), A 350,000 year summer-monsoon multi-proxy stack from the Owen Ridge, Northern Arabian Sea, *Marine Geology, 201*, 35–51, doi:10.1016/S0025-3227(03)00207-X.
Crowley, T. J. (1983), Depth-dependent carbonate dissolution changes in the eastern North Atlantic during the last 170,000 years, *Mar. Geol.*, *54*, 25–31.
de Villiers, S. (2004), Optimum growth conditions as opposed to calcite saturation as a control on the calcification rate and shell-weight of marine foraminifera, *Mar. Biol.*, *144*(1), 45–49, doi:10.1007/s00227-003-1183-8.
de Villiers, S., M. Greaves, and H. Elderfield (2002), An intensity ratio calibration method for the accurate determination of Mg/Ca and Sr/Ca of marine carbonates by ICP-AES, *Geochem. Geophys. Geosyst.*, *3*(1), 1001, doi:10.1029/2001GC000169.
Dekens, P. S., D. W. Lea, D. K. Pak, and H. J. Spero (2002), Core top calibration of Mg/Ca in tropical foraminifera: Refining paleotemperature estimation, *Geochem. Geophys. Geosyst.*, *3*(4), 1022, doi:10.1029/2001GC000200.
Duplessy, J.-C., J. L. Blanc, and A. W. H. Bé (1981), Oxygen-18 enrichment of planktonic foraminifera due to gametogenetic calcification below the euphotic zone, *Science*, *213*, 1247–1250.
Elderfield, H., M. Vautravers, and M. Cooper (2002), The relationship between shell size and Mg/Ca, Sr/Ca, d18O and d13C of species of planktic foraminifera, *Geochem. Geophys. Geosyst.*, *3*(8), 1052, doi:10.1029/2001GC000194.
Emeis, K.-C., D. M. Anderson, H. Doose, D. Kroon, and D. Schulz-Bull (1995), Sea-surface temperatures and the history of monsoon upwelling in the northwest Arabian Sea during the last 500,000 years, *Quat. Res.*, *43*, 355–361.
Emerson, S., and M. Bender (1981), Carbon fluxes at the sediment water interface of the deep-sea: Calcium carbonate preservation, *J. Mar. Res.*, *39*, 139–162.
Fehrenbacher, J., P. A. Martin, and G. Eshel (2006), Glacial deep water carbonate chemistry inferred from foraminiferal Mg/Ca: A case study from the western tropical Atlantic, *Geochem. Geophys. Geosyst.*, *7*, Q09P16, doi:10.1029/2005GC001156.
Friedrich, O., R. Schiebel, P. A. Wilson, S. Weldeab, C. J. Beer, M. J. Cooper, and K. Fiebig (2012), Influence of test size, water depth and ecology on Mg/Ca. Sr/Ca, d18O and d13C in nine modern species of planktic foraminifers, *Earth Planet. Sci. Lett.*, *319–320*, 133–145.
Gillooly, J. F., E. L. Charnov, G. B. West, V. M. Savage, and J. H. Brown (2002), Effects of size and temperature on developmental time, *Nature*, *417*, 70–73.
Gonzalez-Mora, B., F. J. Sierro, and J. A. Flores (2008), Controls of shell calcification in planktonic foraminifers, *Quat. Sci. Rev.*, *27*, 956–961.
Govin, A., E. Michel, L. Labeyrie, C. Waelbroeck, F. Dewilde, and E. Jansen (2009), Evidence for northward expansion of Antarctic Bottom Water mass in the Southern Ocean during the last glacial inception, *Paleoceanography*, *24*, PA1202, doi:10.1029/2008PA001603.
Greaves, M., S. Barker, C. Daunt, and H. Elderfield (2005), Accuracy, standardization, and interlaboratory calibration standards for foraminiferal Mg/Ca thermometry, *Geochem. Geophys. Geosyst.*, *6*, Q02D13, doi:10.1029/2004GC000790.
Hales, B., and S. Emerson (1997), Calcite dissolution in sediments of the Ceara Rise: In Situ measurements of porewater O_2, pH, and CO_2(aq), *Geochim. Cosmochim. Acta*, *61*(3), 501–514.
Hastings, D. W., A. D. Russell, and S. R. Emerson (1998), Foraminiferal magnesium in Globeriginoides sacculifer as a paleotemperature proxy, *Paleoceanography*, *13*(2), 161–169.
Hemleben, C., M. Spindler, and O. R. Anderson (Eds.) (1989), *Modern Planktonic Foraminifera*, 363 pp., Springer, New York.
Hodell, D. A., C. D. Charles, and F. J. Sierro (2001), Late Pleistocene evolution of the ocean's carbonate system, *Earth Planet. Sci. Lett.*, *192*, 109–124.
Howard, W. R., and W. L. Prell (1994), Late Quaternary $CaCO_3$ production and preservation in the Southern Ocean: Implications for oceanic and atmospheric carbon cycling, *Paleoceanography*, *9*(3), 453–482.

Johnstone, H. J. H., M. Schulz, S. Barker, and H. Elderfield (2010), Inside story: An X-ray computed tomography method for assessing dissolution in the tests of planktonic foraminifera, *Mar. Micropaleontol.*, *77*, 58–70.
Johnstone, H. J. H., M. Schulz, J. Yu, and H. Elderfield (2011), Calibrating computed tomography based dissolution index XDX to dissolution bias of Mg/Ca in planktic foraminifera, *Paleoceanography*, *26*, PA1215, doi:10.1029/2009PA001902.
Key, R. M., A. Kozyr, C. L. Sabine, K. Lee, R. Wanninkhof, J. L. Bullister, R. A. Feely, F. J. Millero, C. Mordy, and T.-H. Peng (2004), A global ocean carbon climatology: Results from Global Data Analysis Project (GLODAP), *Global Biogeochem. Cycles*, *18*, GB4031, doi:10.1029/2004GB002247.
Kiefer, T., and M. Kienast (2005), Patterns of deglacial warming in the Pacific Ocean: A review with emphasis on the time interval of Heinrich event 1, *Quat. Sci. Rev.*, *24*, 1063–1081.
Kiefer, T., I. N. McCave, and H. Elderfield (2006), Antarctic control on tropical Indian Ocean sea surface temperature and hydrography, *Geophys. Res. Lett.*, *33*, L24612, doi:10.1029/2006GL027097.
Kloecker, R., T. S. Ivanochko, G.-J. Brummer, S. J. A. Jung, G. Ganssen, D. Kroon, R. S. Ganeshram, and R. Henrich (2007), Variation in production, input and preservation of metastable calcium carbonate off Somalia during the last 90,000 years, *Quat. Sci. Rev.*, *26*, 2674–2683.
Le, J., and N. J. Shackleton (1992), Carbonate dissolution fluctuations in the western equatorial Pacific during the late Quaternary, *Paleoceanography*, *7*(1), 21–42.
Lea, D. W., D. K. Pal, and H. J. Spero (2000), Climate impact of late quaternary equatorial pacific sea surface temperature variations, *Science*, *289*, 1719–1724, doi:10.1126/science.289.5485.1719.
Leuschner, D. C., and F. Sirocko (2000), The low-latitude monsoon climate during Dansgaard-Oeschger cycles and Heinrich Events, *Quat. Sci. Rev.*, *19*, 243–254.
Lisiecki, L., and M. Raymo (2005), A Pliocene-Pleistocene stack of 57 globally distributed benthic D18O records, *Paleoceanography*, *20*, PA1003, doi:10.1029/2004PA001071.
Locarnini, R. A., A. V. Mishonov, J. I. Antonov, T. P. Boyer, and H. E. Garcia (2006), World Ocean Atlas 2005, in *Temperature*, vol. *1*, *NOAA Atlas NESDIS 61*, edited by S. Levitus, 182 pp., U.S. Gov. Print. Off., Washington, D. C.
Lohmann, G. P. (1995), A model for variation in the chemistry of planktonic foraminifera due to secondary calcification and selective dissolution, *Paleoceanography*, *10*(3), 445–458, doi:10.1029/95PA00059.
Marchitto, T. M., J. Lynch-Stieglitz, and S. R. Hemming (2005), Deep Pacific $CaCO_3$ compensation and glacial-interglacial atmospheric CO_2, *Earth Planet. Sci. Lett.*, *231*, 317–336.
McCave, I. N. (2001), RRS Charles Darwin Cruise, *Rep. 129*, Dep. of Earth Sci., Univ. of Cambridge, UK.
McCave, I. N., T. Kiefer, D. R. Thornalley, and H. Elderfield (2005), Deep flow in the Madagascar-Marscarene Basin over the last 150,000 years, *Philos. Trans. R. Soc. B*, *363*, 81–99.
Mekik, F., and L. Ratterink (2008), Effects of surface ocean conditions on deep-sea calcite dissolution proxies in the tropical Pacific, *Paleoceanography*, *23*, PA1216, doi:10.1029/2007PA001433.
Mekik, F. A., R. F. Anderson, P. Loubere, R. Francois, and M. Richaud (2012), The mystery of the missing deglacial carbonate preservation maximum, *Quat. Sci. Rev.*, *39*, 60–72.
Merkel, U., M. Prange, and M. Schulz (2010), ENSO variability and teleconnections during glacial climates, *Quat. Sci. Rev.*, *29*, 86–100.
Mohtadi, M., A. Lueckge, S. Steinke, J. Groeneveld, D. Hebbeln, and N. Westphal (2010), Late Pleistocene surface and thermocline conditions of the eastern tropical Indian Ocean, *Quat. Sci. Rev.*, *29*, 887–896.
Moy, A. D., W. R. Howard, S. G. Bray, and T. W. Trull (2009), Reduced calcification in modern Southern Ocean planktonic foraminifera, *Nat. Geosci.*, *2*, 276–280, doi:10.1038/ngeo460.
Naik, S. S., and P. D. Naidu (2007), Calcite dissolution along a transect in the western tropical Indian Ocean: A multiproxy approach, *Geochem. Geophys. Geosyst.*, *8*, Q08009, doi:10.1029/2007GC001615.
Naik, S. S., P. D. Naidu, P. Govil, and S. Godad (2010), Relationship between weights of planktonic foraminifer shell and surface water $[CO_3^{2-}]$ concentration during the Holocene and last Glacial period, *Mar. Geol.*, *275*(1–4), 278–282.
Nuernberg, D., A. Mueller, and R. R. Schneider (2000), Paleo-sea surface temperature calculations in the equatorial east Atlantic from Mg/Ca ratios in planktic foraminifera: A comparison to sea surface temperature estimates from UK'37, oxygen isotopes, and foraminiferal transfer function, *Paleoceanography*, *15*(1), 124–134.
Pierrot, D. E. Lewis, and D. W. R. Wallace (2006), MS Excel Program Developed for CO2 System Calculations. ORNL/CDIAC-105a. Carbon Dioxide Information Analysis Center, Oak Ridge National Laboratory, U.S. Department of Energy, Oak Ridge, Tennessee. doi: 10.3334/CDIAC/otg.CO2SYS_XLS_CDIAC105a.
Petit, J. R., et al. (1999), Climate and atmospheric history of the past 420,000 years from the Vostok ice core, Antarctica, *Nature*, *399*, 429–436, doi:10.1038/20859.
Regenberg, M., D. Nürnberg, S. Steph, J. Groeneveld, D. Garbe-Schönberg, R. Tiedemann, and W.-C. Dullo (2006), Assessing the effect of dissolution on planktonic foraminiferal Mg/Ca ratios: Evidence from Caribbean core tops, *Geochem. Geophys. Geosyst.*, *7*, Q07P15, doi:10.1029/2005GC001019.
Regenberg, M., S. Steph, D. Nuernberg, R. Tiedemann, and D. Garbe-Schoenberg (2009), Calibrating Mg/Ca ratios of multiple planktonic foraminiferal species with d18O-calcification temperatures: Paleothermometry for the upper water column, *Earth Planet. Sci. Lett.*, *278*, 324–336.
Romahn, S., A. Mackensen, J. Groeneveld, and J. Pätzold (2013), Deglacial intermediate water reorganization: New evidence from the Indian Ocean, *Clim. Past Discuss.*, *9*, 4035–4063, doi:10.5194/cpd-9–4035-2013.
Rosenthal, Y., G. P. Lohmann, K. C. Lohmann, and R. M. Sherrell (2000), Incorporation and preservation of Mg in Globigerinoides sacculifer: Implications for reconstructing the temperature and 18O/16O of seawater, *Paleoceanography*, *15*(1), 135–145.
Rosenthal, Y., et al. (2004), Interlaboratory comparison study of Mg/Ca and Sr/Ca measurements in planktonic foraminifera for paleoceanographic research, *Geochem. Geophys. Geosyst.*, *5*, Q04D09, doi:10.1029/2003GC000650.
Rostek, F., G. Ruhland, F. C. Bassinot, P. J. Mueller, L. D. Labeyrie, Y. Lancelot, and E. Bard (1993), Reconstructing sea surface temperature and salinity using δ18O and alkenone records, *Nature*, *364*, 319–321.
Rostek, F., E. Bard, L. Beaufort, C. Sonzogni, and G. Ganssen (1997), Sea surface temperature and productivity records for the past 240 kyr in the Arabian Sea, *Deep Sea Res., Part II*, *44*(6–7), 1461–1480.
Saraswat, R., R. Nigam, S. Weldeab, A. Mackensen, and P. D. Naidu (2005), A first look at past sea surface temperatures in the equatorial Indian Ocean from Mg/Ca in foraminifera, *Geophys. Res. Lett.*, *32*, L24605, doi:10.1029/2005GL024093.
Saraswat, R., D. Lea, R. Nigam, A. Mackensen, and D. K. Naik (2013), Deglaciation in the tropical Indian Ocean driven by interplay between the regional monsoon and global teleconnections, *Earth Planet. Sci. Lett.*, *375*, 166–175, doi:10.1016/j.epsl.2013.05.022i.

Sarnthein, M., K. Winn, S. J. A. Jung, J.-C. Duplessy, L. Labeyrie, H. Erlenkeuser, and G. Ganssen (1994), Changes in East Atlantic deepwater circulation over the last 30,000 years: Eight time slice reconstructions, *Paleoceanography*, *9*(2), 209–267.

Schlitzer, R., (2002), Interactive analysis and visualization of geoscience data with ocean data view, *Computers & Geosciences, 28*(10), 1211-1218. Schlitzer, R., Ocean Data View, http://odv.awi.de, 2012.

Schott, F. A., M. Dengler, and R. Schoenefeldt (2002), The shallow overturning circulation of the Indian Ocean, *Prog. Oceanogr.*, *53*, 57–103.

Schott, F. A., S.-P. Xie, and J. P. McCreary Jr. (2009), Indian Ocean circulation and climate variability, *Rev. Geophys.*, *47*, RG1002, doi:10.1029/2007RG000245.

Shackleton, N. J., and E. Vincent (1978), Oxygen and carbon isotope studies in recent foraminifera from the Southwest Indian Ocean, *Mar. Micropaleontol.*, *3*, 1–13.

Sigman, D. M., and E. A. Boyle (2000), Glacial/interglacial variations in atmospheric carbon dioxide, *Nature*, *407*, 859–869.

Slutz, R. J., S. J. Lubker, J. D. Hiscox, S. D. Woodruff, R. L. Jenne, D. H. Joseph, P. M. Steuer, and J. D. Elms (1985), *Comprehensive Ocean-Atmosphere Data Set: Release 1*, Climate Research Program, Boulder, Colorado. http://web1.cdc.noaa.gov/coads/Release_1/coads.html.

Spero, H. J., J. Bijma, D. W. Lea, and B. E. Bemis (1997), Effect of seawater carbonate concentration on foraminiferal carbon and oxygen isotopes, *Nature*, *390*(4), 497–500.

Yu, J., W. S. Broecker, H. Elderfield, J. Zhangdong, J. McManus, and F. Zhang (2010), Loss of carbon from the deep sea since the Last Glacial Maximum, *Science*, *330*, 1084–1087, doi:10.1126/science.1193221.

Zeebe, R., and D. Wolf-Gladrow (2001), *CO_2 in Seawater: Equilibrium, Kinetics, Isotopes. Elsevier Oceanography. Ser.*, vol. *65*, edited by D. Halpern, Elsevier, Amsterdam, pp.346.